J. Fluid Mech. (2013), *vol.* 730, *pp.* 392–418.
doi:10.1017/jfm.2013.303

Unsteady three-dimensional sources in deep water with an elastic cover and their applications

Izolda V. Sturova†

Lavrentyev Institute of Hydrodynamics, av. Lavrentyev 15, 630090 Novosibirsk, Russia

(Received 20 September 2012; revised 17 May 2013; accepted 9 June 2013;
first published online 1 August 2013)

The velocity potential is derived for a transient source of arbitrary strength undergoing arbitrary three-dimensional motion. The initially quiescent fluid of infinite depth is assumed to be inviscid, incompressible and homogeneous. The upper surface of the fluid is covered by a thin layer of elastic material of uniform density with lateral stress. The linearized initial boundary-value problem is formulated within the framework of the potential-flow theory, and the Laplace transform technique is employed to obtain the solution. The potential of a time-harmonic source with forward speed is obtained as a particular case. The far-field wave motion at long time is determined via the method of stationary phase. The problems of radiation (surge, sway and heave) of the flexural–gravity waves by a submerged sphere advancing at constant forward speed are investigated. The method of multipole expansions is used. Numerical results are obtained for the wave-making resistance and lift, added-mass and damping coefficients. The effects of an ice sheet and broken ice on the hydrodynamic loads are discussed in detail.

Key words: elastic waves, ice sheets, waves/free-surface flows

1. Introduction

Within the framework of linear theory, knowledge of the velocity potential due to fundamental singularities moving under a free surface allows one to tackle the problem of wave generation by a partially immersed or completely submerged body (e.g. Wehausen & Laitone 1960). In the same way, it is possible to determine the wave motion in a more complicated case when the upper boundary of the fluid has an elastic cover of infinite extent. Wave motion due to fundamental line and point singularities with time-dependent strength submerged in a fluid with an elastic cover and/or an inertial surface has been investigated in recent years. Basically, two kinds of unsteady problems were considered: instantaneous or time-harmonic singularities with fixed location. Chowdhury & Mandal (2006) analytically derived the velocity potentials for the motion due to fundamental singularities in the forms of two-dimensional line source, line multipoles and three-dimensional point multipoles submerged in a fluid of uniform finite depth. The generation of unsteady waves by concentrated disturbances in infinitely deep water was studied by Lu & Dai (2006, 2008*a*) for an elastic cover and an inertial surface, respectively. The inertial surface represents the effect of a thin uniform distribution of non-interacting floating matter. Fluid of finite depth, covered by

† Email address for correspondence: sturova@hydro.nsc.ru

a thin elastic plate or by an inertial surface with capillary effect, was considered by Lu & Dai (2008*b*). In these three papers, the asymptotic representations of the wave motion for long time with a fixed distance-to-time ratio were derived with the method of stationary phase.

The study of wave problems in water covered by a thin elastic sheet has considerable practical importance in application to natural and man-made systems such as ice sheets and very large floating structures (VLFS) like oil storage bases, offshore pleasure cities, floating airport runways, etc. Considerable attention has been paid to three-dimensional flexural oscillations of an ice sheet due to a moving pressure area (e.g. Kheysin 1967; Squire *et al.* 1996; Bukatov & Zharkov 1997). In contrast, studies of the ice-cover effect on the motion of a submerged body have been carried out only recently. The radiation problem at zero forward speed for a sphere submerged in a uniform and two-layer fluid have been considered by Das & Mandal (2008, 2010) and Mohapatra & Bora (2010). The added-mass and damping coefficients for a sphere in heave and sway motion were obtained for a range of key parameters such as wavenumber, submersion depths of the sphere, and flexural rigidity of the ice cover. The radiation problem for forced oscillations of a submerged body is similar to the diffraction problem of the scattering of periodic waves incident on a fixed body. Das & Mandal (2006, 2007) studied the oblique incidence of waves on a horizontal circular cylinder submerged in a uniform and a two-layer fluid. In the latter case, an external disturbance can be caused by both surface and internal waves. Scattering of water waves by a sphere and wave-induced exciting forces were studied by Mohapatra & Bora (2012). The two-dimensional problem of small oscillations of a horizontal cylinder of arbitrary cross-section submerged in a linearly stratified fluid of finite depth was studied by Sturova (2011). The added-mass and damping coefficients were calculated as a function of the oscillation frequency for the case of an ice sheet and for three special cases: broken ice, free surface and rigid lid.

The translating motion of a submerged body under ice cover was studied numerically and experimentally by Kozin, Chizhumov & Zemlyak (2010). The deflections and the strains in the ice cover were computed for an elongated body using the finite element method in combination with the boundary element method. The influence of the thickness of continuous ice cover on its stress–strain state and the possibility of dynamic destruction of the ice cover by a moving submerged body were studied. Unsteady horizontal motion of a slender body was studied by Pogorelova, Kozin & Zemlyak (2012). The submerged body was simulated by a prescribed source–sink system. It was shown that the destruction of the ice cover by a moving slender body is possible in limited ranges of ice thickness, depth of the body and its velocity. The wave patterns generated by a steadily moving submerged sphere in deep water under ice cover were considered by Sturova (2012). The steady hydrodynamic load (wave resistance and lift) acting on the body and the ice-cover deformations were determined. The generation of the flexural–gravity waves by a two-dimensional dipole situated under the ice sheet in a fluid of infinite depth was investigated by Savin & Savin (2012) and Il'ichev, Savin & Savin (2012). The impulsive start of a horizontal uniform motion of the dipole was considered. As is well known, the two-dimensional dipole is a model of a circular cylinder moving in a fluid. In spite of the extensive literature on flexural–gravity waves, in the author's opinion, the effect of the ice cover on the motion of a submerged body has still not been fully elucidated.

In this paper, the velocity potential of a transient three-dimensional source of arbitrary strength and in arbitrary motion is derived. A thin elastic plate of infinite extent with lateral stress is assumed to cover the upper surface of the fluid domain.

The initially quiescent fluid of infinite depth is assumed to be inviscid, incompressible and homogeneous. This velocity potential is fundamental to the analysis of various types of body motion under the influence of waves. Other sources can be obtained from this source by specifying the appropriate strength and motion, among them the sources that were considered by Chowdhury & Mandal (2006) and Lu & Dai (2006, 2008*a*,*b*). The case of a translating and oscillating source is considered in more detail. The basic properties of the wave motion in the far field are determined. This information is used for the solution of the radiation problem for a submerged sphere at forward speed by the multipole expansion method based on the results by Wu (1995) for a free surface. Numerical results are obtained for the hydrodynamic load: wave resistance and lift, added masses and damping coefficients.

2. Mathematical formulation

Consider a fixed, rectangular coordinate system $Oxyz$, where the (xy)-plane coincides with the undisturbed upper surface of the fluid, and the positive z-axis points upwards. The initially quiescent fluid of infinite depth is assumed to be inviscid, incompressible and homogeneous. The upper surface is covered by a thin layer of elastic material of uniform density with lateral stress. The motion of the fluid is generated due to a point-mass source of time-dependent strength, which starts operating at time $t = 0$. The linearized initial- and boundary-value problem is formulated within the framework of potential flow. The position of a source and its strength at time $t \geqslant 0$ are given by $\boldsymbol{\xi}(t) = (\xi(t), \eta(t), \zeta(t))$ and $\mu(t)$, where $\zeta(t) < 0$ and $\mu(t) = 0$ for $t < 0$. This transient source is the most general source.

The motion of the fluid can be described by a velocity potential $\Phi(\boldsymbol{x}, t)$ $(t > 0)$. In the linear theory, Φ satisfies, in the fluid domain,

$$\Delta\Phi = \mu(t)\delta(\boldsymbol{x} - \boldsymbol{\xi}(t)), \quad -\infty < x, y < \infty, \quad z < 0, \tag{2.1}$$

where Δ denotes the three-dimensional Laplace operator, $\boldsymbol{x} = (x, y, z)$ and δ is the Dirac delta-function.

If $w(x, y, t)$ denotes a small vertical displacement of the upper surface from its equilibrium position, then the linearized kinematic and dynamic conditions at the upper surface are given by

$$\partial w/\partial t = \partial\Phi/\partial z, \quad D\Delta_2^2 w + Q\Delta_2 w + M\partial^2 w/\partial t^2 + \rho\partial\Phi/\partial t + g\rho w = 0, \quad z = 0, \tag{2.2}$$

where $D = Eh_1^3/[12(1-\nu^2)]$, $M = \rho_1 h_1$, $\Delta_2 \equiv \partial^2/\partial x^2 + \partial^2/\partial y^2$, ρ is the density of the fluid, g is the acceleration of gravity, E is the Young's modulus for the elastic cover, Q is its lateral stress (with compression at $Q > 0$ and stretch at $Q < 0$), and ν, ρ_1 and h_1 are the Poisson's ratio, density and thickness of the elastic cover, respectively. Moreover, since the disturbance must vanish at infinity, it is required that

$$\lim_{z\to-\infty} \nabla\Phi = 0, \quad \lim_{R\to\infty} \nabla\Phi = 0 \ (t \geqslant 0), \quad R^2 = (x - \xi(t))^2 + (y - \eta(t))^2. \tag{2.3}$$

The initial conditions at $z = 0$ are

$$\Phi = w = \partial w/\partial t = 0, \quad t = 0. \tag{2.4}$$

The first equation in (2.2) implies that there is no cavitation between the elastic plate and the fluid surface.

There are some particular cases of this problem, which are presented in table 1. If the elastic parameter D is zero, but $Q = -T$ $(T > 0)$, then the plate-covered surface reduces to a flexible membrane. If, in addition, the surface density of the plate $M = 0$,

Flexible membrane	$D=0, \quad Q=-T \quad (T>0)$
Free surface with surface tension	$D=M=0, \quad Q=-T \quad (T>0)$
Inertial surface	$D=Q=0$
Usual free surface	$D=Q=M=0$

TABLE 1. The particular cases of the problem considered.

then the upper boundary of the fluid becomes a free surface with surface tension and T is called the coefficient of surface tension. As $D=Q=0$, the plate-covered surface reduces to an inertial surface, which represents the effect of a thin uniform distribution of non-interacting floating matter, for example, broken ice (e.g. Lu & Dai 2008*b*). If, in addition, also $M=0$, then the upper boundary of the fluid becomes the usual free surface.

The initial-value problem (2.1)–(2.4) is solved by the standard method. The solution of this problem can be written as

$$\Phi=\chi+\phi, \quad \chi=\mu(t)(r_1^{-1}-r_2^{-1}), \quad r_{1,2}^2=R^2+(z\mp\eta(t))^2. \tag{2.5}$$

The governing equation for ϕ is now simply the Laplace equation

$$\Delta\phi=0, \quad -\infty<x,y<\infty, \quad z<0, \tag{2.6}$$

and the initial conditions, obtained by inserting (2.5) into (2.4), are

$$\phi=\partial\phi/\partial t=0, \quad z=0, \ t=0. \tag{2.7}$$

In order to obtain the formal solution for the harmonic function $\phi(\boldsymbol{x},t)$, it is convenient to introduce the Laplace transform with respect to t. Let us assume that $\bar{f}(\boldsymbol{x},s)$ denotes the Laplace transform of the function $f(\boldsymbol{x},t)$ in the form

$$\bar{f}(\boldsymbol{x},s)=\int_0^\infty f(\boldsymbol{x},t)\mathrm{e}^{-st}\,\mathrm{d}t, \quad s>0. \tag{2.8}$$

Taking the Laplace transform for the boundary conditions (2.2) and using the initial conditions (2.7), we obtain

$$(D\Delta_2^2+Q\Delta_2+s^2M+g\rho)\frac{\partial\bar{\phi}}{\partial z}+\rho s^2\bar{\phi}=-(D\Delta_2^2+Q\Delta_2+s^2M+g\rho)\frac{\partial\bar{\chi}}{\partial z}, \quad z=0. \tag{2.9}$$

From the well-known representation of r^{-1} (e.g. Gradshteyn & Ryzhik 1980, 6.611 and 3.937),

$$\frac{1}{\sqrt{x^2+y^2+z^2}}=\frac{1}{2\pi}\int_{-\infty}^\infty\int_{-\infty}^\infty\frac{\mathrm{e}^{-k|z|}}{k}\mathrm{e}^{\mathrm{i}(k_1x+k_2y)}\,\mathrm{d}k_1\,\mathrm{d}k_2, \quad k^2=k_1^2+k_2^2, \tag{2.10}$$

we can write

$$\chi(\boldsymbol{x},t)=\frac{\mu(t)}{2\pi}\int_{-\infty}^\infty\int_{-\infty}^\infty\frac{1}{k}[\mathrm{e}^{-k|z-\zeta(t)|}-\mathrm{e}^{-k|z+\zeta(t)|}]\mathrm{e}^{\mathrm{i}[k_1(x-\xi(t))+k_2(y-\eta(t))]}\,\mathrm{d}k_1\,\mathrm{d}k_2, \tag{2.11}$$

which leads to

$$\left.\frac{\partial\bar{\chi}}{\partial z}\right|_{z=0}=-\frac{1}{\pi}\int_0^\infty\mu(t)\mathrm{e}^{-st}\int_{-\infty}^\infty\int_{-\infty}^\infty\mathrm{e}^{k\zeta(t)+\mathrm{i}[k_1(x-\xi(t))+k_2(y-\eta(t))]}\,\mathrm{d}k_1\,\mathrm{d}k_2\,\mathrm{d}t. \tag{2.12}$$

We seek the solution for $\bar{\phi}(\bar{x}, s)$ in the form

$$\bar{\phi} = \int_{-\infty}^{\infty}\int_{-\infty}^{\infty} \Omega(k_1, k_2, z, s)\mathrm{e}^{\mathrm{i}(k_1 x + k_2 y)}\,\mathrm{d}k_1\,\mathrm{d}k_2. \tag{2.13}$$

Substituting this relation in (2.6) and using the boundary condition in (2.3) as $z \to -\infty$, we have $\Omega(k_1, k_2, z, s) = \mathrm{e}^{kz}F(k_1, k_2, s)$. The function $F(k_1, k_2, s)$ is determined from (2.9) in the form

$$\left.\begin{aligned} F &= \frac{\Lambda(k) + s^2 M}{\pi(\rho + kM)[s^2 + \omega^2(k)]}\int_0^{\infty} \mu(t)\mathrm{e}^{k\zeta(t) - \mathrm{i}[k_1\xi(t) + k_2\eta(t)] - st}\,\mathrm{d}t, \\ \Lambda(k) &= Dk^4 - Qk^2 + g\rho, \end{aligned}\right\} \tag{2.14}$$

where

$$\omega(k) = \sqrt{k\Lambda(k)/(\rho + kM)}. \tag{2.15}$$

Equation (2.15) is the dispersion relation for the flexural–gravity waves at infinite depth of fluid. This function determines the wavenumber k for a specified frequency ω.

Taking the inverse Laplace transform of (2.13), we obtain

$$\phi = \frac{1}{\pi}\int_{-\infty}^{\infty}\int_{-\infty}^{\infty}\frac{1}{\rho + kM}\int_0^{\infty} \mu(\tau)\mathrm{e}^{k(z+\zeta(\tau)) + \mathrm{i}[k_1(x-\xi(\tau)) + k_2(y-\eta(\tau))]}\Upsilon(k_1, k_2, t, \tau)\,\mathrm{d}\tau\,\mathrm{d}k_1\,\mathrm{d}k_2, \tag{2.16}$$

where

$$\Upsilon = \frac{1}{2\pi\mathrm{i}}\int_{\sigma-\mathrm{i}\infty}^{\sigma+\mathrm{i}\infty}\frac{\Lambda(k) + s^2 M}{s^2 + \omega^2(k)}\mathrm{e}^{s(t-\tau)}\,\mathrm{d}s. \tag{2.17}$$

The value σ is chosen so that the integration path in (2.17) is situated from the right of all singularities that represent the roots of the equation $s^2 + \omega^2(k) = 0$. It is clear that this equation has only two pure imaginary roots $s = \pm\mathrm{i}\omega(k)$. The function Υ is different from zero only at $t > \tau$ and is equal to

$$\Upsilon(k_1, k_2, t, \tau) = \frac{\rho\Lambda(k)\sin[\omega(t-\tau)]}{\omega(k)(\rho + kM)}. \tag{2.18}$$

Further, if the following integral representation of the zeroth-order Bessel function of the first kind J_0 is used (e.g. Wehausen & Laitone 1960, p. 491)

$$\mathrm{J}_0(kR(\tau)) = \frac{1}{2\pi}\int_{-\pi}^{\pi}\mathrm{e}^{\mathrm{i}k[(x-\xi(\tau))\cos\theta + (y-\eta(\tau))\sin\theta]}\,\mathrm{d}\theta, \tag{2.19}$$

the function $\phi(\boldsymbol{x}, t)$ can be written as

$$\phi = 2\rho\int_0^t \mu(\tau)\int_0^{\infty}\frac{\omega(k)}{\rho + Mk}\mathrm{e}^{k(z+\zeta(\tau))}\mathrm{J}_0(kR(\tau))\sin(\omega(k)(t-\tau))\,\mathrm{d}k\,\mathrm{d}\tau. \tag{2.20}$$

If $D = Q = M = 0$, this solution is consistent with the velocity potential for the usual free surface and coincides with the result given by Wehausen & Laitone (1960, equation (13.49)).

It is known that the dispersion relation (2.15) imposes a limitation on the compressive force Q. The condition $Q < Q_* \equiv 2\sqrt{g\rho D}$ ensures the stability of the floating elastic plate (e.g. Kheysin 1967). In the present analysis, it is assumed also

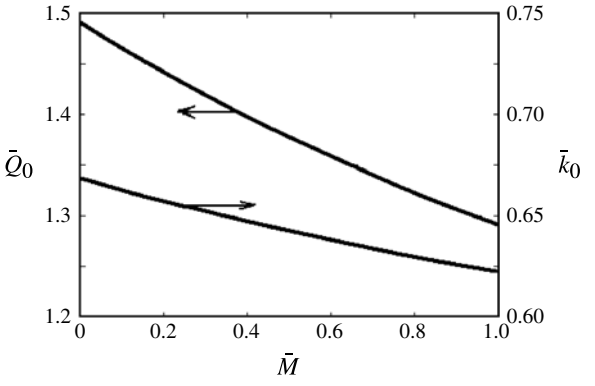

FIGURE 1. Dependence of $\bar{Q}_0$ and $\bar{k}_0$ on $\bar{M}$.

that $Q < Q_0 < Q_*$, where Q_0 is defined by the condition of a positive group velocity $c_g(k) = \mathrm{d}\omega/\mathrm{d}k$ for all wavenumbers $k \geqslant 0$. The method of evaluation of Q_0 was given by Bukatov (1980) for a fluid of finite depth. The value Q_0 and its associated wavenumber k_0 are found from the two equations $c_g(k_0) = 0$ and $\mathrm{d}c_g(k)/\mathrm{d}k|_{k=k_0} = 0$. For deep water, the value k_0 is determined as the positive root of the polynomial

$$Dk_0^4(8Mk_0 + 15\rho) - 3g\rho^2 = 0 \tag{2.21}$$

and the value Q_0 is equal to

$$Q_0 = \frac{Dk_0^4(4Mk_0 + 5\rho) + g\rho^2}{k_0^2(2Mk_0 + 3\rho)}. \tag{2.22}$$

At $M = 0$, the non-dimensional values $\bar{k}_0 = k_0(D/g\rho)^{1/4}$ and $\bar{Q}_0 = Q_0/\sqrt{g\rho D}$ are determined explicitly: $\bar{k}_0 = 5^{-1/4} \approx 0.669$, $\bar{Q}_0 = \sqrt{20}/3 \approx 1.491$. Figure 1 shows the non-dimensional values $\bar{Q}_0$ and $\bar{k}_0$ as functions of $\bar{M} = M/(g/\rho^3 D)^{1/4}$. It can be seen that the values k_0 and Q_0 decrease with increasing M.

All particular cases of the upper cover can be divided into two groups. For an inertial surface and the usual free surface, both the phase and group velocities decrease monotonically from infinity to zero with increasing wavenumber. For an elastic cover, a flexible membrane and a free surface with surface tension, both the phase $c_f(k) = \omega/k$ and group velocities $c_g(k)$ have minimal values, denoted by $U_f = c_f(k_f)$ and $U_g = c_g(k_g)$, respectively. Here k_f corresponds to the wavenumber at which $\mathrm{d}c_f(k)/\mathrm{d}k|_{k=k_f} = 0$, and analogously $k_g < k_f$ is defined by the equation $\mathrm{d}c_g(k)/\mathrm{d}k|_{k=k_g} = 0$. The wavenumber k_f is the positive root of the polynomial

$$Dk_f^4(2Mk_f/\rho + 3) - Qk_f^2 - 2gMk_f - g\rho = 0. \tag{2.23}$$

According to (2.15), the minimal phase velocity U_f is equal to

$$U_f = \sqrt{\Lambda(k_f)/[k_f(\rho + Mk_f)]}. \tag{2.24}$$

The value k_g is determined as the positive root of the 10th-degree polynomial

$$\begin{aligned} &Dk_g^5[4DM(2Mk_g + 5\rho)k_g^4 + C_1k_g^3 - 28\rho QMk_g^2 + C_2k_g + 48g\rho^2M] \\ &+ C_3k_g^4 - g\rho^2(4QMk_g^3 + 6\rho Qk_g^2 + 4g\rho Mk_g + g\rho^2) = 0, \end{aligned} \tag{2.25}$$

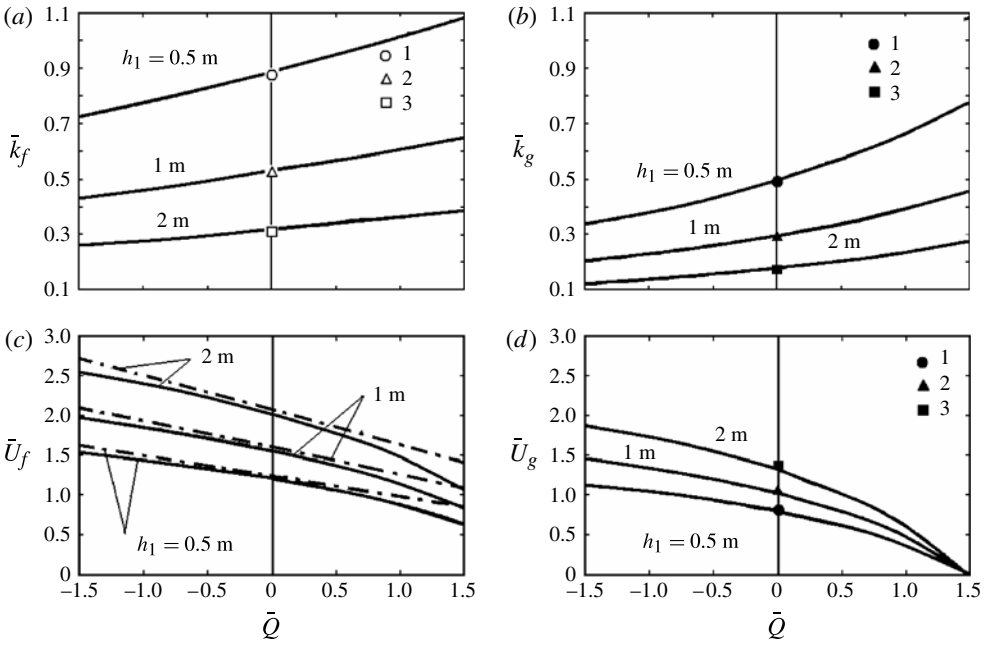

FIGURE 2. The wavenumbers (*a*) $\bar{k}_f$ and (*b*) $\bar{k}_g$ plotted against $\bar{Q}$ for different values of h_1. The open and filled symbols represent $\bar{k}_f$ and $\bar{k}_g$ at $Q = M = 0$ and, respectively: 1, $h_1 = 0.5$ m; 2, $h_1 = 1$ m; 3, $h_1 = 2$ m. The velocities (*c*) $\bar{U}_f$ and (*d*) $\bar{U}_g$ plotted against $\bar{Q}$ for different values of h_1. Dash-dotted lines represent the approximate solution (A 3) for U_f at small stress. The filled symbols represent $\bar{U}_g$ at $Q = M = 0$ and, respectively: 1, $h_1 = 0.5$ m; 2, $h_1 = 1$ m; 3, $h_1 = 2$ m.

where

$$\left.\begin{aligned} &C_1 = 3(5\rho^2 D - 4QM^2), \quad C_2 = 2\rho(12gM^2 - 11\rho Q), \\ &C_3 = \rho(30g\rho^2 D + 3\rho Q^2 - 4gQM^2). \end{aligned}\right\} \tag{2.26}$$

The minimal group velocity U_g is equal to

$$U_g = \frac{\rho(5Dk_g^4 - 3Qk_g^2 + g\rho) + 2Mk_g^3(2Dk_g^2 - Q)}{2(\rho + Mk_g)^{3/2}\sqrt{k_g \Lambda(k_g)}}. \tag{2.27}$$

For special cases (see table 1), the values k_f, k_g and U_f, U_g are defined in the Appendix.

Figure 2(*a*,*b*) shows the non-dimensional values $(\bar{k}_f, \bar{k}_g) = a(k_f, k_g)$ calculated from equations (2.23) and (2.25), respectively, as functions of the non-dimensional lateral stress $\bar{Q} = Q/\sqrt{g\rho D}$ for the case of ice cover. The following input data are used:

$$E = 5 \text{ GPa}, \quad \nu = 0.3, \quad \rho = 1025 \text{ kg m}^{-3}, \quad \rho_1 = 922.5 \text{ kg m}^{-3} \tag{2.28}$$

at an ice thickness of $h_1 = 0.5,\ 1,\ 2$ m. The value $a = 10$ m is the scale of length. The open symbols 1, 2, 3 denote the values of $\bar{k}_f$ at $Q = M = 0$ in (A 2) for $h_1 = 0.5,\ 1,\ 2$ m, respectively. The filled symbols denote similar values $\bar{k}_g$ in (A 5). Figure 2(*c*,*d*) shows the influence of the lateral stress on the minimal values of the

phase and group velocities $(\bar{U}_f, \bar{U}_g) = (U_f, U_g)/\sqrt{ag}$ calculated from (2.24) and (2.27), respectively, for different values of ice thickness. The dash-dotted lines correspond to $\bar{U}_f$ given by (A 3) for small lateral stress. The filled symbols 1, 2, 3 denote the values $\bar{U}_g$ given by (A 5) at $Q = M = 0$ for the different values of h_1. The magnitude of $\bar{Q}$ characterizing the ice compression (stretch) is changed within the following limits: $-1.5 \leqslant \bar{Q} \leqslant 1.5$. As seen from figure 2(*a*,*b*), the wavenumbers k_f and k_g decrease with increasing ice thickness and increase with lateral stress, whereas the opposite behaviour takes place for minimal phase and group velocities U_f and U_g. Note that the realistic ice lateral stress is small (e.g. Schulkes, Hosking & Sneyd 1987) and can be taken as $Q = 0$. However, the lateral stress may be important for artificial floating platforms. It is known that the solutions of the hydroelastic problem for sea ice and VLFS in many cases are similar (Squire 2008).

3. Velocity potential of translating and oscillating source

The total velocity potential (2.5) with the function $\phi(\boldsymbol{x}, t)$ in the form (2.20) can be applied to different particular cases by prescribing the special choice of $\mu(t)$ and the motion of the source. Thus, if

$$\mu(t) = \mu_0 \cos \sigma t \quad \text{and} \quad \boldsymbol{\xi} \text{ is fixed}, \tag{3.1}$$

one has the potential function for a stationary source of oscillating strength, switched on impulsively at $t = 0$. If one takes

$$\mu(t) = \mu_0, \quad \xi(t) = \xi_0 + ut, \quad \eta(t) = \eta_0, \quad \zeta(t) = \zeta_0, \tag{3.2}$$

one obtains the velocity potential for a source that is switched on at $t = 0$ and afterwards moves uniformly in the direction Ox. These two cases may be combined by choosing the source strength in the form (3.1) and its motion in the form (3.2). For finite t, the velocity potential of a time-harmonic source with forward speed in a coordinate system moving with velocity u in direction Ox ($\bar{x} = x - ut$) is given by

$$\Phi(\bar{x}, y, z, t) = \mu_0 \cos \sigma t \, (r_1^{-1} - r_2^{-1}) + \phi(\bar{x}, y, z, t), \tag{3.3}$$

where, from an integral representation J_0 in (2.19),

$$\phi = 4 \int_0^{\pi/2} \int_0^t \cos \sigma (t - \tau) \int_0^\infty \mathscr{F}(k, \gamma) \cos(k \cos \gamma (X + u\tau)) \sin(\omega(k)\tau) \, \mathrm{d}k \, \mathrm{d}\tau \, \mathrm{d}\gamma, \tag{3.4a}$$

$$\mathscr{F}(k, \gamma) = \frac{\mu_0 \rho \omega(k)}{\pi(\rho + kM)} \mathrm{e}^{k(z+\zeta_0)} \cos(kY \sin \gamma), \quad X = \bar{x} - \xi_0, \ Y = y - \eta_0, \tag{3.4b}$$

and the range of the γ integration is reduced in the quadrant $[0, \pi/2]$. Using the function-product relations for sine and cosine, (3.4*a*) becomes

$$\phi = \int_0^{\pi/2} \int_0^t \int_0^\infty \mathscr{F}(k, \gamma)(\sin \Psi_1 + \sin \Psi_2 + \sin \Psi_3 + \sin \Psi_4) \, \mathrm{d}k \, \mathrm{d}\tau \, \mathrm{d}\gamma, \tag{3.5}$$

where

$$\Psi_{1,2}(k,\tau,\gamma)=[\omega(k)+\sigma]\tau\pm k(X+u\tau)\cos\gamma-\sigma t, \tag{3.6a}$$

$$\Psi_{3,4}(k,\tau,\gamma)=[\omega(k)-\sigma]\tau\pm k(X+u\tau)\cos\gamma+\sigma t. \tag{3.6b}$$

As $t\to\infty$, the principal physical features of the wave motion in the far field can be determined by the asymptotic analysis of the double integral for k and τ in (3.5) using the method of stationary phase (e.g. Born & Wolf 1964, Appendix III). An especially important role is played by the critical (stationary) points at which

$$\partial\Psi_n/\partial k=\partial\Psi_n/\partial\tau=0\quad(n=1,\dots,4). \tag{3.7}$$

The fulfilment of these equations permits the determination of the wavenumbers and the direction of propagation for the waves in the far field.

The function Ψ_1 has no points of stationary phase in the integration angle range $[0,\pi/2]$ because the partial derivative

$$\partial\Psi_1/\partial\tau=\omega(k)+\sigma+kU,\quad U=u\cos\gamma, \tag{3.8}$$

has no zeros in this range. The function Ψ_2 has no more than two critical points. The equation

$$\omega(k)+\sigma-kU=0 \tag{3.9}$$

has two roots denoted by $k_2^{(1)}$ and $k_2^{(2)}$, with $k_2^{(1)}<k_2^{(2)}$ only if $u>U_1(\sigma)=c_g(k_1^*)$ and $0<\gamma<\gamma_1$, where the wavenumber k_1^* satisfies the equation $kc_g(k)-\omega(k)=\sigma$ and $\gamma_1=\arccos(U_1/u)$. It follows from the dispersion relation (2.15) that $k_1^*\to k_f$ and $U_1\to U_f$ at $\sigma\to 0$. If the conditions mentioned above do not hold, the function Ψ_2 has no critical points. The values $k_2^{(i)}$ $(i=1,2)$ are defined as the positive roots of the polynomial

$$Dk^5-(Q+MU^2)k^3-U(\rho U-2\sigma M)k^2+(\rho g+2\rho\sigma U-\sigma^2M)k-\rho\sigma^2=0 \tag{3.10}$$

satisfying (3.9). The direction of propagation for these waves is determined from the fulfilment of the equality

$$\partial\Psi_2/\partial k=(c_g(k)-U)\tau-X\cos\gamma=0. \tag{3.11}$$

The waves corresponding to $k_2^{(i)}$ $(i=1,2)$ propagate upstream $(X>0)$ at $c_g(k_2^{(i)})-U>0$ and downstream $(X<0)$ at $c_g(k_2^{(i)})-U<0$.

The function Ψ_3 always has only one critical point. The equation

$$\omega(k)-\sigma+kU=0 \tag{3.12}$$

has one zero k_3 for any $\gamma\in[0,\pi/2]$. The value k_3 is defined as the positive root of the polynomial (3.10) satisfying (3.12). The waves corresponding to the wavenumber k_3 always propagate downstream.

The function Ψ_4 has no more than three critical points. The equation

$$\omega(k)-\sigma-kU=0 \tag{3.13}$$

always has one root $k_4^{(1)}$ and two additional roots $k_4^{(2)}$ and $k_4^{(3)}$ only at $\sigma<\sigma^*\equiv\omega(k_g)-k_gU_g$ and $U_3<U<U_2$. The functions $U_2(\sigma)$ and $U_3(\sigma)$ are determined as follows: $U_2=c_g(k_2^*)$ and $U_3=c_g(k_3^*)$. Here the values $k_2^*<k_g<k_3^*$ are the roots of the equation

$$\omega(k)-kc_g(k)=\sigma. \tag{3.14}$$

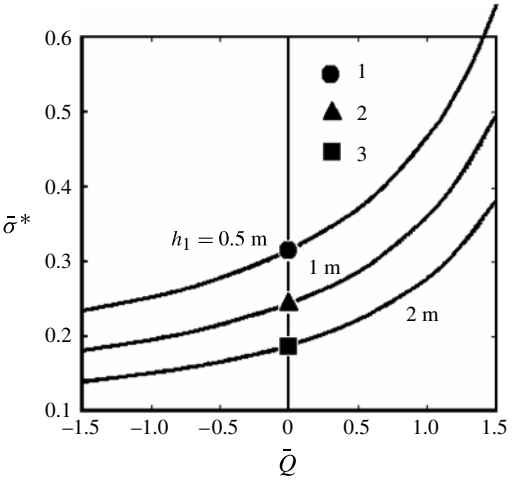

FIGURE 3. The influence of lateral stress on the non-dimensional frequency $\bar{\sigma}^*$ for different values of h_1. The symbols 1, 2, 3 represent the values of $\bar{\sigma}^*$ at $Q = M = 0$ for $h_1 = 0.5,\ 1,\ 2$ m, respectively.

It follows from the dispersion relation (2.15) that $k_2^* \to 0$, $k_3^* \to k_f$ and $U_2 \to \infty$, $U_3 \to U_f$ at $\sigma \to 0$, but $k_2^*, k_3^* \to k_g$ and $U_2, U_3 \to U_g$ at $\sigma \to \sigma^*$. If, for given $\sigma < \sigma^*$, the velocity $u > U_2(\sigma)$, three roots exist for $\gamma_2 < \gamma < \gamma_3$; however, if $U_3(\sigma) < u < U_2(\sigma)$, then three roots exist only for $0 < \gamma < \gamma_3$, where $\gamma_2 = \arccos(U_2/u)$ and $\gamma_3 = \arccos(U_3/u)$. The values $k_4^{(j)}$ $(j = 1, 2, 3)$ are determined as the positive roots of the polynomial

$$Dk^5 - (Q + MU^2)k^3 - U(\rho U + 2\sigma M)k^2 + (\rho g - 2\rho\sigma U - \sigma^2 M)k - \rho\sigma^2 = 0 \quad (3.15)$$

satisfying (3.13). The waves corresponding to the wavenumbers $k_4^{(j)}$ propagate upstream if $c_g(k_4^{(j)}) - U > 0$ and downstream otherwise.

The behaviour of the values k_f, U_f and k_g, U_g for the ice cover with the input data (2.28) is shown in figure 2(*a–d*). The influence of the lateral stress on the non-dimensional frequency $\bar{\sigma}_* = \sigma_* \sqrt{a/g}$ at different values of ice thickness is illustrated in figure 3. The frequency increases with the lateral stress and decreases with the ice thickness. The symbols 1, 2, 3 represent the values $\bar{\sigma}_*$ at $Q = M = 0$ for $h_1 = 0.5,\ 1,\ 2$ m, respectively.

Figure 4(*a*) shows the variation of U_j $(j = 1, 2, 3)$ with σ for the ice cover with the input data (2.28), $Q = 0$ and $h_1 = 0.5$ m. The curves U_1, U_2, U_3 divide the (σU)-plane into four regions G_n $(n = 1, \ldots, 4)$. All six waves are present in the far field for values σ and U from the region G_1: $k_2^{(1)}$, $k_2^{(2)}$, k_3, $k_4^{(1)}$, $k_4^{(2)}$, $k_4^{(3)}$. There are four waves for the regions G_2 and G_3: $k_2^{(1)}$, $k_2^{(2)}$, k_3, $k_4^{(1)}$ and k_3, $k_4^{(1)}$, $k_4^{(2)}$, $k_4^{(3)}$, respectively. There are only two waves for the region G_4: k_3, $k_4^{(1)}$. Figure 4(*b*) represents the similar picture for capillary–gravity waves, where the input data for water at 20 °C are used: $T = 0.0728$ N m^{-1}, $\rho = 998$ kg m^{-3}.

The basic properties of the flexural–gravity waves generated by oscillating pressure moving over the ice plate were investigated by Bukatov & Cherkesov (1977), Bukatov (1980) and Bukatov & Yaroshenko (1986) for two- and three-dimensional problems and a fluid of finite depth. In this paper, these results for the kinematic properties of

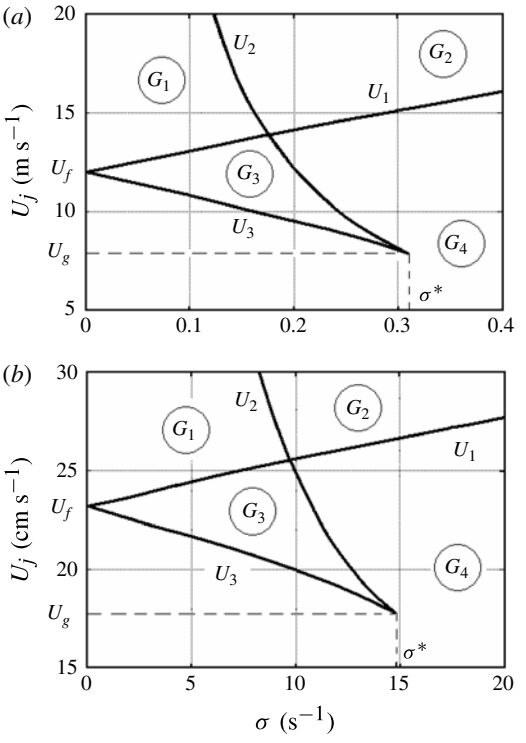

FIGURE 4. Dependence of U_j $(j = 1, 2, 3)$ on the frequency for (a) flexural–gravity waves and (b) capillary–gravity waves.

the far-field waves are presented in simpler form for deep water. It should be noted that the properties of these waves do not depend on the location of the disturbance: on the upper surface, inside the fluid or on the bottom.

For an inertial surface $(D = Q = 0)$, the function Ψ_2 has only one critical point, because in this case (3.9) has one root k_2 for any $\gamma \in [0, \pi/2]$. As before, the function Ψ_3 has only one critical point. The value of k_3 is always less than that of k_2. For Ψ_4, there are two critical points for certain values of γ only at $\sigma < \sigma_{cr} \equiv \sqrt{g\rho/M}$. In this case, (3.13) has two roots $k_4^{(1)}$ and $k_4^{(2)}$, with $k_4^{(1)} < k_4^{(2)}$ at $U < U^* = c_g(k_4^*)$, where k_4^* is the root of (3.14). The value k_4^* is defined as the positive root of the polynomial

$$M^2(g\rho - \sigma^2 M)k^3 + \rho M(g\rho - 3\sigma^2 M)k^2 + 0.25\rho^2(g\rho - 12\sigma^2 M)k - \rho^3\sigma^2 = 0 \quad (3.16)$$

satisfying (3.14). For $u < U^*$, both $k_4^{(1)}$ and $k_4^{(2)}$ exist for $\gamma \in [0, \pi/2]$. However, when $u > U^*$, $k_4^{(1)}$ and $k_4^{(2)}$ exist only for $\gamma > \arccos(U^*/u)$. For the usual free surface $(D = Q = M = 0)$, we have the well-known result: $k_4^* = 4\sigma^2/g$, $U^* = 0.25g/\sigma$. The influence of the frequency σ on the non-dimensional parameter $\sigma U^*/g$ for broken ice with the values ρ and ρ_1 from (2.28) at different values of ice thickness $h_1 = 0.5,\ 1,\ 2$ m is illustrated in figure 5. There are four waves for the region G_1, i.e. $k_2,\ k_3,\ k_4^{(1)},\ k_4^{(1)}$, and only two waves $k_2,\ k_3$ exist for the region G_2.

Consider next the properties of the wave motion in the far field for the particular cases of the problem analysed. At $u = 0$, a source of oscillating strength has a fixed position. In this case, for the elastic cover, the functions Ψ_1 and Ψ_2 have no critical

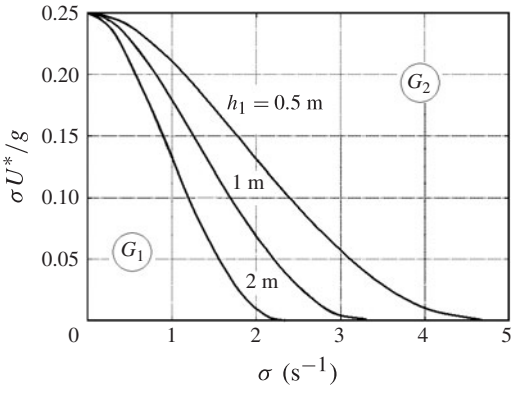

FIGURE 5. The non-dimensional parameter $\sigma U^*/g$ plotted against the frequency σ for different thicknesses of broken ice: $h_1 = 0.5,\ 1,\ 2$ m.

points, but each of the functions Ψ_3 and Ψ_4 always have one critical point, k_3 and k_4, respectively, with $k_3 = k_4$. The wave corresponding to the wavenumber k_3 always propagates downstream, whereas the wave k_4 propagates upstream. For the inertial surface ($D = Q = 0$), progressive waves in the far field do not exist at $M > 0$ and $\sigma > \sigma_{cr}$.

At $\sigma = 0$, the source of fixed strength moves horizontally with constant velocity. In this case, for the elastic cover, the functions Ψ_1 and Ψ_3 have no critical points, but both the functions Ψ_2 and Ψ_4 have no more than two coinciding critical points $k_2^{(1)} = k_3^{(1)}$ and $k_2^{(2)} = k_3^{(2)}$, with $k_2^{(1)} < k_2^{(2)}$. These points exist only if $u > U_f$ and $0 < \gamma < \gamma_0$, where $\gamma_0 = \arccos(U_f/u)$. These values are determined from the equation $c_f(k) = U$, as evident from (3.9). It is well known (e.g. Squire *et al.* 1996) that the group velocity of the flexural–gravity waves exceeds the phase velocity at shorter wavelength (large wavenumber), but is less than the phase speed at longer wavelength (small wavenumber). Accordingly, the waves corresponding to the wavenumbers $k_2^{(1)}$ and $k_3^{(1)}$ always propagate downstream, whereas the waves associated with $k_2^{(2)}$ and $k_3^{(2)}$ propagate upstream. For the inertial surface ($D = Q = 0$), both the functions Ψ_2 and Ψ_4 always have only one critical point, k_2 and k_4, respectively, which are equal to

$$k_2 = k_4 = \begin{cases} (\sqrt{\rho^2 U^2 + 4g\rho M} - \rho U)/(2UM), & M > 0, \\ g/U^2, & M = 0. \end{cases} \tag{3.17}$$

In this case, the phase velocity of any wave exceeds its group velocity, and the gravity waves in the far field always propagate downstream. The foregoing analysis is necessary, in particular, for the solution of the wave radiation problem of a submerged body with forward speed.

4. Wave radiation by a submerged sphere at forward speed

Consider the radiation problem for a submerged sphere of radius a advancing at constant forward speed u. The coordinate system $Oxyz$ is moving with the sphere with the same speed, and x points in the direction of u. The centre of the sphere is located at $x = y = 0,\ z = -h\ (h > 0)$. We also define a spherical coordinate system (r, θ, β)

with the origin fixed at the position of the centre of the sphere:

$$x = r\sin\theta\cos\beta, \quad y = r\sin\theta\sin\beta, \quad z = r\cos\theta - h. \tag{4.1}$$

The total potential Φ may be expanded as

$$\Phi(x, y, z, t) = u[\bar{\phi}(x, y, z) - x] + \mathrm{Re}\left[\sum_{j=1}^{3} \eta_j \phi_j(x, y, z)\exp(\mathrm{i}\sigma t)\right], \tag{4.2}$$

where $\bar{\phi}$ is the steady potential due to unit forward speed, and ϕ_j $(j = 1, 2, 3)$ are radiation potentials corresponding to oscillations of the body in three degrees of freedom (surge, sway and heave) with amplitudes η_j and angular frequency σ. Notice that the three-dimensional body in the general case can oscillate with six degrees of freedom, but, evidently, the rotation of a sphere about its centre does not disturb an inviscid fluid.

If w denotes the small vertical displacement of the upper surface from its equilibrium position, then we can write by analogy with (4.2)

$$w(x, y, t) = \bar{w}(x, y) + \mathrm{Re}\left[\sum_{j=1}^{3} \eta_j w_j(x, y)\exp(\mathrm{i}\sigma t)\right]. \tag{4.3}$$

The velocity potential $\Phi(x, y, z, t)$ should satisfy the Laplace equation in the fluid domain. In the frame of reference moving with the sphere at constant speed u, the boundary conditions (2.2) at the upper surface $(z = 0)$ change to

$$\left(\frac{\partial}{\partial t} - u\frac{\partial}{\partial x}\right) w = \frac{\partial \Phi}{\partial z}, \tag{4.4}$$

$$D\Delta_2^2 w + Q\Delta_2 w + M\left(\frac{\partial}{\partial t} - u\frac{\partial}{\partial x}\right)^2 w + \rho\left(\frac{\partial}{\partial t} - u\frac{\partial}{\partial x}\right)\Phi + g\rho w = 0. \tag{4.5}$$

Using the expansions (4.2) and (4.3), we have at $z = 0$

$$\frac{\partial \bar{w}}{\partial x} = -\frac{\partial \bar{\phi}}{\partial z}, \quad \left(D\Delta_2^2 + Q\Delta_2 + Mu^2\frac{\partial^2}{\partial x^2} + g\rho\right)\frac{\partial \bar{\phi}}{\partial z} + \rho u^2\frac{\partial^2 \bar{\phi}}{\partial x^2} = 0, \tag{4.6}$$

$$\left(\mathrm{i}\sigma - u\frac{\partial}{\partial x}\right) w_j = \frac{\partial \phi_j}{\partial z}, \quad \left[D\Delta_2^2 + Q\Delta_2 + M\left(\mathrm{i}\sigma - u\frac{\partial}{\partial x}\right)^2 + g\rho\right] w_j + \rho\left(\mathrm{i}\sigma - u\frac{\partial}{\partial x}\right)\phi_j = 0. \tag{4.7}$$

The boundary conditions on the body surface S $(r = a)$ are

$$\partial\bar{\phi}/\partial n = n_1, \quad \partial\phi_j/\partial n = \mathrm{i}\sigma n_j + u m_j \quad (j = 1, 2, 3), \tag{4.8}$$

where

$$(n_1, n_2, n_3) = (n_x, n_y, n_z), \quad (m_1, m_2, m_3) = -(\boldsymbol{n}\cdot\nabla)\nabla(\bar{\phi} - x). \tag{4.9}$$

Here $\boldsymbol{n} = (n_x, n_y, n_z)$ is the inward normal of the body surface S. Also, the condition at large depth is

$$\lim_{z\to-\infty} \nabla\Phi = 0. \tag{4.10}$$

Traditionally, to make the problem unique, a radiation condition is implemented, which requires that only the outgoing wave with group velocity larger than the forward speed

can be found far in front of the body. However, we do not need the radiation condition when considering the radiation problem as the limit of the unsteady problem as $t \to \infty$. It is known that the radiation condition in the frequency domain results from the causality condition, which is not needed when solving a time-dependent problem. The asymptotic analysis for the unsteady solution makes it possible to determine the wave motion in the far field at long time.

The hydrodynamic force $\boldsymbol{F}$ acting on the sphere is equal to $\boldsymbol{F} = \int_S P\boldsymbol{n}\,\mathrm{d}s$, where $P(x, y, z, t)$ is the hydrodynamic pressure in the fluid (i.e. the full pressure with the hydrostatic pressure removed). This can be obtained from Euler's integral (e.g. Wehausen & Laitone 1960, p. 461) as

$$P = -\rho\left(\frac{\partial \Phi}{\partial t} + \frac{|\nabla\Phi|^2}{2}\right). \tag{4.11}$$

The hydrodynamic moment about the centre of the sphere is zero.

Using the expansion (4.2), we can write

$$\boldsymbol{F} = \boldsymbol{F}^{(st)} + \mathrm{Re}[\boldsymbol{F}^{(r)}\exp(\mathrm{i}\sigma t)], \tag{4.12}$$

where $\boldsymbol{F}^{(st)}$ and $\boldsymbol{F}^{(r)}$ are the steady and radiation forces, respectively. The value of $\boldsymbol{F}^{(st)}$ is equal to

$$\boldsymbol{F}^{(st)} = -\frac{1}{2}\rho u^2 \int_S \nabla(\bar{\phi} - x)\nabla(\bar{\phi} - x)\boldsymbol{n}\,\mathrm{d}s. \tag{4.13}$$

We denote the x-, y-, z-components of $\boldsymbol{F}^{(st)}$ as F_1, F_2, F_3. The components of the radiation force $\boldsymbol{F}^{(r)}$ can be represented as

$$\boldsymbol{F}_i^{(r)} = \sum_{j=1}^{3}\eta_j\tau_{ij}, \quad \tau_{ij} = -\rho\int_S[\mathrm{i}\sigma\phi_j + u\nabla(\bar{\phi} - x)\nabla\phi_j]n_i\,\mathrm{d}s \quad (i = 1, 2, 3). \tag{4.14}$$

The multipole expansion method (Wu 1995) is used to solve the problem considered. We write the steady potential $\bar{\phi}(x, y, z)$ in terms of the following expansion based on associated Legendre functions P_n^m:

$$\bar{\phi} = \sum_{n=0}^{\infty}\sum_{m=0}^{n}\bar{A}_n^m\left[\frac{a^{n+1}}{r^{n+1}}\mathrm{P}_n^m(\cos\theta)\cos m\beta + \frac{a^{n+1}\mathrm{i}^m}{2\pi(n-m)!}\int_{-\pi}^{\pi}\int_L \frac{T_1}{Z_1}V\cos m\gamma\,\mathrm{d}k\,\mathrm{d}\gamma\right], \tag{4.15}$$

where

$$T_1(k, \gamma) = Z_1(k, \gamma) + 2\rho u^2 k\cos^2\gamma, \quad Z_1(k, \gamma) = \Lambda(k) - k(\rho + Mk)u^2\cos^2\gamma, \tag{4.16a}$$

$$V(k, \gamma) = k^n\exp[k(z - h + \mathrm{i}(x\cos\gamma + y\sin\gamma))]. \tag{4.16b}$$

Here the first term in the square brackets in (4.15) is for the sphere in an unbounded fluid domain and the second term is introduced to satisfy the conditions (4.3) and (4.10).

The integration route L in (4.15) is from zero to infinity. There are singularities in the integrand. Using the results of § 3 for a source of fixed strength moving horizontally with constant speed, it can be easily shown that the equation $Z_1(k, \gamma) = 0$ has two positive roots $k_2^{(1)}$ and $k_2^{(2)}$ if $u|\cos\gamma| > U_f$. For convenience, we introduce the notation $\kappa_1 = k_2^{(1)}$ and $\kappa_2 = k_2^{(2)}$. The integration route L should pass over the singularity κ_1 and under the singularity κ_2 when $|\gamma| < \pi/2$, and vice versa when $|\gamma| > \pi/2$.

By applying the condition on the body surface (4.8) for the steady potential and following the approach of Wu (1995), we obtain the system of linear algebraic equations for determination of unknown coefficients $\bar{A}_n^m$:

$$\frac{n+1}{a}\bar{A}_n^m + \frac{n\varepsilon_m}{2\pi}\sum_{n'=0}^{\infty}\sum_{m'=0}^{n'}\frac{a^{n+n'}}{(n+m)!(n'-m')!}I_0(m',n',m,n)\bar{A}_{n'}^{m'} = \delta_{n1}\delta_{m1}, \qquad (4.17)$$

where $\varepsilon_0 = 1$ and $\varepsilon_m = 2$ if $m > 0$, δ_{ij} is the Kronecker delta-function,

$$I_0(m,n,m',n') = -(-1)^{(m-m')/2}4\int_0^{\pi/2}\mathrm{pv}\int_0^{\infty}k^{n+n'}\mathrm{e}^{-2kh}\cos m\gamma\cos m'\gamma\frac{T_1(k,\gamma)}{Z_1(k,\gamma)}\,\mathrm{d}k\,\mathrm{d}\gamma \qquad (4.18)$$

if $m - m'$ is even and

$$I_0(m,n,m',n') = (-1)^{(m-m'-1)/2}4\pi\int_0^{\gamma_0}\cos m\gamma\cos m'\gamma\sum_{j=1}^{2}(-1)^j\kappa_j^{n+n'}\mathrm{e}^{-2\kappa_j h}\frac{T_1(\kappa_j,\gamma)}{Z_1'(\kappa_j,\gamma)}\,\mathrm{d}\gamma \qquad (4.19)$$

if $m - m'$ is odd. Here the notation pv indicates the principal-value integration, $Z_1'(\kappa_j,\gamma) \equiv \partial Z_1/\partial k|_{k=\kappa_j}$ $(j = 1, 2)$ and the value γ_0 is defined as

$$\gamma_0 = \begin{cases} 0, & u < U_f, \\ \arccos(U_f/u), & u > U_f. \end{cases} \qquad (4.20)$$

For an inertial surface ($D = Q = 0$), the equation $Z_1(k,\gamma) = 0$ has only one positive root at all values of the speed u. In this case, the second term in the sum of (4.19) should be omitted and the value of γ_0 in (4.20) is equal to $\pi/2$. Note that there is an explicit solution for this root in accordance with (3.17) and the integration over k in (4.18) can be calculated using the exponential integral (e.g. Wu & Eatock Taylor 1988).

The solution of (4.17) may be obtained by truncating the infinite series at a finite number $n = N$, depending on the accuracy required. Once the solution is found, the components of the steady hydrodynamic force in (4.13) can be obtained. Using the results given by Wu (1995), we have

$$F_j = \frac{1}{2}\rho u^2\int_S(\bar{\phi} - x)m_j\,\mathrm{d}s \quad (j = 1, 2, 3), \qquad (4.21)$$

where

$$F_1 = -2\rho\pi u^2\left[\sum_{n=1}^{\infty}\sum_{m=0}^{n}\frac{1}{\varepsilon_m}\frac{n+2}{n+1}\frac{(n+m+2)!}{(n-m)!}\bar{A}_n^m\bar{A}_{n+1}^{m+1} - \sum_{n=2}^{\infty}\sum_{m=0}^{n-2}\frac{1}{\varepsilon_m}\frac{n+1}{n}\frac{(n+m)!}{(n-m-2)!}\bar{A}_n^m\bar{A}_{n-1}^{m+1}\right], \qquad (4.22)$$

$$F_3 = 4\rho\pi u^2\sum_{n=1}^{\infty}\sum_{m=0}^{n}\frac{1}{\varepsilon_m}\frac{n+2}{n+1}\frac{(n+m+1)!}{(n-m)!}\bar{A}_n^m\bar{A}_{n+1}^m. \qquad (4.23)$$

As a consequence of the symmetry of the sphere, we have $F_2 = 0$. The solution of the steady problem is described in more detail in Sturova (2012).

The multipole expansion for the radiation potential $\phi_j(x, y, z)$ has the form

$$\phi_j = \sum_{n=0}^{\infty}\sum_{m=0}^{n} A_n^m \left[\frac{a^{n+1}}{r^{n+1}}\mathrm{P}_n^m(\cos\theta)\cos m\beta + \frac{a^{n+1}\mathrm{i}^m}{2\pi(n-m)!}\int_{-\pi}^{\pi}\int_L \frac{T_2}{Z_2}V\cos m\gamma\,\mathrm{d}k\,\mathrm{d}\gamma\right] + \sum_{n=0}^{\infty}\sum_{m=0}^{n} B_n^m \left[\frac{a^{n+1}}{r^{n+1}}\mathrm{P}_n^m(\cos\theta)\sin m\beta + \frac{a^{n+1}\mathrm{i}^m}{2\pi(n-m)!}\int_{-\pi}^{\pi}\int_L \frac{T_2}{Z_2}V\sin m\gamma\,\mathrm{d}k\,\mathrm{d}\gamma\right], \tag{4.24}$$

where

$$T_2(k,\gamma) = Z_2(k,\gamma) + 2\rho(\sigma - uk\cos\gamma)^2, \tag{4.25a}$$

$$Z_2(k,\gamma) = k\Lambda(k) - (\sigma - uk\cos\gamma)^2(\rho + Mk). \tag{4.25b}$$

Both integrands are singular in (4.24) when the equation $Z_2(k,\gamma) = 0$ is satisfied. The function $Z_2(k,\gamma)$ can be represented in the form

$$Z_2(k,\gamma) = (\rho + Mk)[\omega(k) - \sigma + uk\cos\gamma][\omega(k) + \sigma - uk\cos\gamma]. \tag{4.26}$$

Therefore, at $|\gamma| < \pi/2$, the zeros of the function $Z_2(k,\gamma)$ coincide with the critical points of the functions Ψ_2 and Ψ_3, defined in § 3. At $|\gamma| > \pi/2$, the zeros of the function $Z_2(k,\gamma)$ coincide with the critical points of the functions Ψ_1 and Ψ_4. The paths at the singularities depend on the direction of propagation for the waves in the far field.

By applying the condition on the body surface (4.8) for the radiation potential, we obtain the system of equations for the unknown coefficients A_n^m and B_n^m:

$$\frac{n+1}{a}A_n^m + \frac{n\varepsilon_m}{2\pi}\sum_{n'=0}^{\infty}\sum_{m'=0}^{n'}\frac{a^{n+n'}(-\mathrm{i})^m\mathrm{i}^{m'}}{(n+m)!(n'-m')!}I_1(m',n',m,n)A_{n'}^{m'} = C_n^m, \tag{4.27}$$

$$B_n^m = 0 \tag{4.28}$$

for surge ($j = 1$);

$$A_n^m = 0, \tag{4.29}$$

$$\frac{n+1}{a}B_n^m + \frac{n\varepsilon_m}{2\pi}\sum_{n'=0}^{\infty}\sum_{m'=0}^{n'}\frac{a^{n+n'}(-\mathrm{i})^m\mathrm{i}^{m'}}{(n+m)!(n'-m')!}I_2(m',n',m,n)B_{n'}^{m'} = D_n^m \tag{4.30}$$

for sway ($j = 2$); and

$$\frac{n+1}{a}A_n^m + \frac{n\varepsilon_m}{2\pi}\sum_{n'=0}^{\infty}\sum_{m'=0}^{n'}\frac{a^{n+n'}(-\mathrm{i})^m\mathrm{i}^{m'}}{(n+m)!(n'-m')!}I_1(m',n',m,n)A_{n'}^{m'} = G_n^m, \tag{4.31}$$

$$B_n^m = 0 \tag{4.32}$$

for heave ($j = 3$). Here

$$I_1(m,n,m',n') = -2\int_0^{\pi}\int_L k^{n+n'}\mathrm{e}^{-2kh}\cos m\gamma\cos m'\gamma\,\frac{T_2}{Z_2}\,\mathrm{d}k\,\mathrm{d}\gamma, \tag{4.33}$$

$$I_2(m,n,m',n') = -2\int_0^{\pi}\int_L k^{n+n'}\mathrm{e}^{-2kh}\sin m\gamma\sin m'\gamma\,\frac{T_2}{Z_2}\,\mathrm{d}k\,\mathrm{d}\gamma, \tag{4.34}$$

$$C_n^m = \mathrm{i}\sigma\delta_{n1}\delta_{m1} + \frac{u}{a^2}\left\{(n+1)\left[\frac{1-\varepsilon_m}{\varepsilon_{m-1}}\bar{A}_{n-1}^{m-1} + \frac{1}{2}(n-m)(n-m-1)\bar{A}_{n-1}^{m+1}\right]\right.$$
$$\left. + \frac{n(n+2)}{n+1}\left[\frac{\varepsilon_m - 1}{\varepsilon_{m-1}}\bar{A}_{n+1}^{m-1} - \frac{1}{2}(n+m+2)(n+m+1)\bar{A}_{n+1}^{m+1}\right]\right\}, \tag{4.35a}$$

$$D_n^m = \mathrm{i}\sigma\delta_{n1}\delta_{m1} - \frac{u}{a^2}(\varepsilon_m - 1)\left\{(n+1)\left[\frac{1}{\varepsilon_{m-1}}\bar{A}_{n-1}^{m-1} + \frac{1}{2}(n-m)(n-m-1)\bar{A}_{n-1}^{m+1}\right]\right.$$
$$\left. - \frac{n(n+2)}{n+1}\left[\frac{1}{\varepsilon_{m-1}}\bar{A}_{n+1}^{m-1} + \frac{1}{2}(n+m+2)(n+m+1)\bar{A}_{n+1}^{m+1}\right]\right\}, \tag{4.35b}$$

$$G_n^m = -\mathrm{i}\sigma\delta_{n1}\delta_{m0} + \frac{u}{a^2}\left[(n-m)(n+1)\bar{A}_{n-1}^m + \frac{n(n+2)}{n+1}(n+m+1)\bar{A}_{n-1}^m\right]. \tag{4.35c}$$

Once the solutions of (4.27), (4.30) and (4.31) are found, the values of τ_{ij}, with the added masses μ_{ij} and the damping coefficients λ_{ij}, can be obtained from (4.14), using the results (Wu 1995)

$$\tau_{ij} = \sigma^2\mu_{ij} - \mathrm{i}\sigma\lambda_{ij} = \rho\int_S \frac{\partial\phi_i^*}{\partial n}\phi_j\,\mathrm{d}s, \tag{4.36}$$

where

$$\tau_{11} = 4\pi\rho a^2\sum_{n=1}^{\infty}\sum_{m=0}^{n}\frac{1}{\varepsilon_m}\frac{1}{2n+1}\frac{(n+m)!}{(n-m)!}C_n^{m*}\left[\frac{2n+1}{n}A_n^m(1) - \frac{a}{n}C_n^m\right], \tag{4.37}$$

$$\tau_{22} = 4\pi\rho a^2\sum_{n=1}^{\infty}\sum_{m=0}^{n}\frac{1}{\varepsilon_m}\frac{1}{2n+1}\frac{(n+m)!}{(n-m)!}D_n^{m*}\left[\frac{2n+1}{n}B_n^m(2) - \frac{a}{n}D_n^m\right], \tag{4.38}$$

$$\tau_{33} = 4\pi\rho a^2\sum_{n=1}^{\infty}\sum_{m=0}^{n}\frac{1}{\varepsilon_m}\frac{1}{2n+1}\frac{(n+m)!}{(n-m)!}G_n^{m*}\left[\frac{2n+1}{n}A_n^m(3) - \frac{a}{n}G_n^m\right], \tag{4.39}$$

$$\tau_{13} = 4\pi\rho a^2\sum_{n=1}^{\infty}\sum_{m=0}^{n}\frac{1}{\varepsilon_m}\frac{1}{2n+1}\frac{(n+m)!}{(n-m)!}C_n^{m*}\left[\frac{2n+1}{n}A_n^m(3) - \frac{a}{n}G_n^m\right], \tag{4.40}$$

$$\tau_{31} = 4\pi\rho a^2\sum_{n=1}^{\infty}\sum_{m=0}^{n}\frac{1}{\varepsilon_m}\frac{1}{2n+1}\frac{(n+m)!}{(n-m)!}G_n^{m*}\left[\frac{2n+1}{n}A_n^m(1) - \frac{a}{n}C_n^m\right], \tag{4.41}$$

while all other hydrodynamic coefficients are zero. Here the symbol * denotes complex conjugate, and $A_n^m(1)$, $B_n^m(2)$ and $A_n^m(3)$ are the solutions of (4.27), (4.30) and (4.31), respectively.

5. Numerical results for the hydrodynamic load

Numerical calculations are performed for ice cover using the input data (2.28). The sphere is submerged at $h = 2a$ and its radius is equal to $a = 10$ m. The results for hydrodynamic load are obtained by taking $N = 5$. It was found that further increase of N does not affect the first four digits after the decimal point.

Figure 6 gives the wave resistance and lift coefficients of a sphere submerged under the usual free surface and broken ice as functions of non-dimensional speed $\bar{u} = u/\sqrt{ga}$. Non-dimensional coefficients are defined from (4.22) and (4.23) as $\bar{F}_1 = -F_1/(\pi g\rho a^3)$ and $\bar{F}_3 = F_3/(\pi\rho a^2u^2)$. The results for the wave resistance in

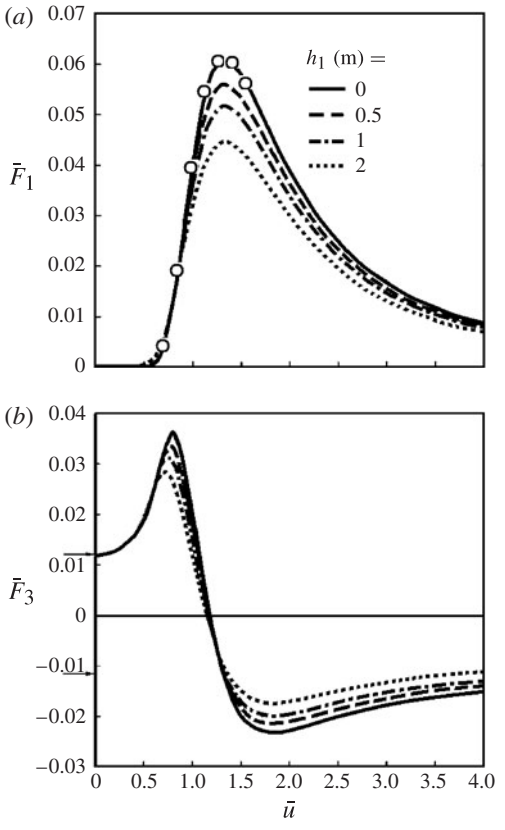

FIGURE 6. The influence of forward speed on the steady hydrodynamic load for the free surface (solid lines) and broken ice (dashed, dash-dotted and dotted lines) at $h_1 = 0.5,\ 1,\ 2$ m, respectively: (*a*) wave resistance and (*b*) lift. Open circles correspond to the results by Wu & Eatock Taylor (1988) for a free surface.

the case of the usual free surface are compared with the values tabulated by Wu & Eatock Taylor (1988), which are shown by open circles in figure 6(*a*). Good agreement is found. In figure 6(*b*), the horizontal arrows indicate the values of the lift for two limiting cases: $u \to 0$ ($\bar{F}_3 = 0.0120$) and $u \to \infty$ ($\bar{F}_3 = -0.0115$). The first case corresponds to a rigid lid on the upper boundary of the water, whereas the second case corresponds to a weightless fluid with free surface. The solutions of the steady problem for these cases can be easily obtained by the multipole expansion method. For the rigid lid, the boundary condition on the upper boundary of the fluid for the steady potential has the form

$$\partial\bar{\phi}/\partial z = 0, \quad z = 0. \tag{5.1}$$

Then we have in (4.15) $T_1/Z_1 = 1$, and in (4.17)

$$I_0(m, n, m', n') = -\frac{2\pi(n+n')!}{\varepsilon_m(2h)^{n+n'+1}}\delta_{mm'}. \tag{5.2}$$

For the weightless fluid with a free surface, the boundary condition has the form

$$\bar{\phi} = 0, \quad z = 0. \tag{5.3}$$

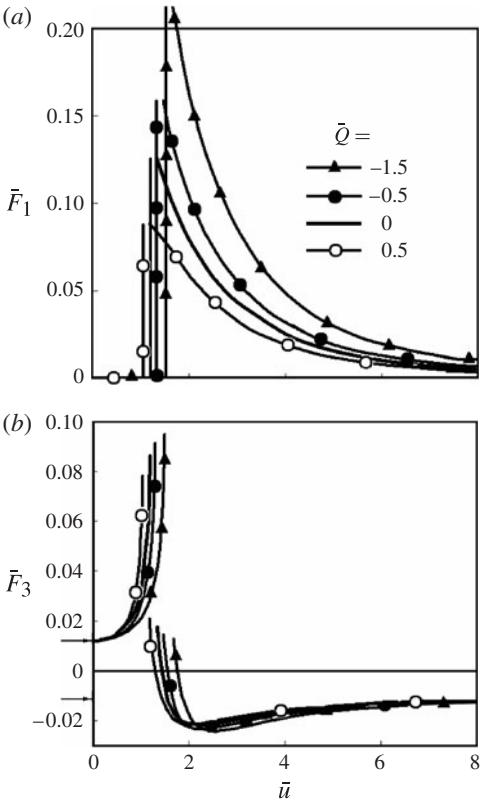

FIGURE 7. Effect of lateral stress of the ice sheet with $h_1 = 0.5$ m on the steady hydrodynamic load: (*a*) wave resistance and (*b*) lift.

Then we have $T_1/Z_1 = -1$ in (4.15), and the relation for $I_0(m, n, m', n')$ coincides with (5.2) taken with inverse sign. Waves are not generated in these two cases and the wave resistance is zero. Figure 6 shows that the maximum values of wave resistance and lift take place for a sphere moving under a free surface. For broken ice, the extreme values of the steady force decrease with increasing ice thickness but the qualitative behaviour of the steady force does not change. It is seen that the lift tends to the value for the rigid-lid condition at the free surface, when the velocity of the sphere tends to zero.

The steady hydrodynamic force for a sphere moving under an ice sheet of thickness $h_1 = 0.5$ m at different values of the lateral stress is shown in figure 7. Both the wave resistance and the lift have discontinuities at $u = U_f$. Similar behaviour of the wave resistance was found by Yeung & Kim (1998) for a moving load on a floating elastic plate. It was shown that the discontinuity of the wave resistance has a finite value. At $u < U_f$, the wave resistance is equal to zero but the lift increases sharply with u. At $u > U_f$, the wave resistance increases with stretching of the ice cover. As in figure 6(*b*), the horizontal arrows in figure 7(*b*) indicate the values of the lift for two limiting cases. The lift coefficient tends to the value for the rigid lid at $u \to 0$ and to the value for the weightless fluid at $u \to \infty$ regardless of the lateral stress.

Figure 8 presents the radiation load, with the added-mass coefficients shown in figure 8(*a–d*) and damping coefficients shown in figure 8(*e–h*), for a sphere

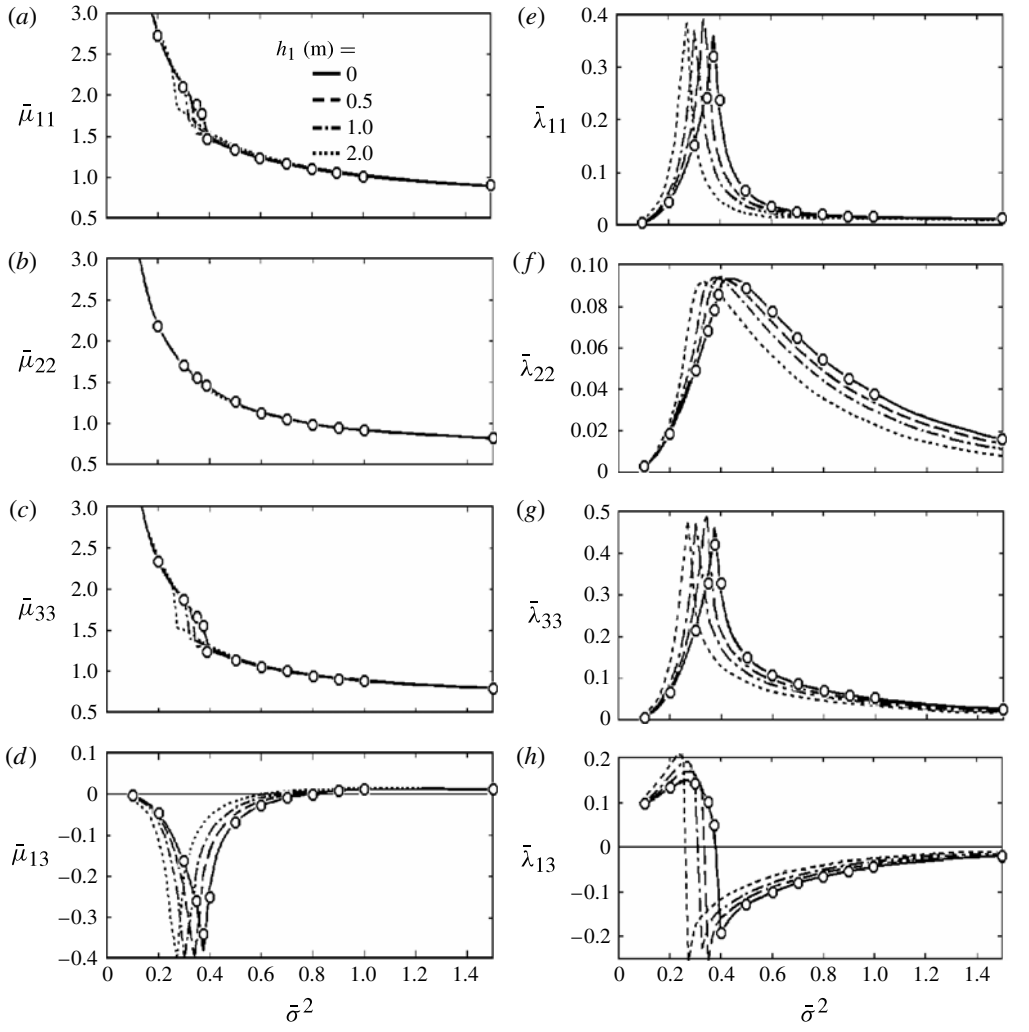

FIGURE 8. The radiation force at $\bar{u} = 0.4$ for a free surface (solid lines) and for broken ice (dashed, dash-dotted and dotted lines) at $h_1 = 0.5,\ 1,\ 2$ m, respectively: (*a*,*e*) surge, (*b*,*f*) sway, (*c*,*g*) heave, (*d*,*h*) surge–heave. Open circles correspond to the results by Wu & Eatock Taylor (1988) for a free surface.

submerged under a free surface and broken ice as functions of non-dimensional frequency $\bar{\sigma}^2 = \sigma^2 a/g$. These results correspond to $\bar{u} = 0.4$. They are obtained from (4.37)–(4.40), with the following normalization:

$$\bar{\mu}_{ij} = \mu_{ij}/(\pi\rho a^3), \quad \bar{\lambda}_{ij} = \lambda_{ij}/(\pi\rho a^3\sigma). \tag{5.4}$$

The results for the free surface are compared with the tabulated values in Wu & Eatock Taylor (1988) and shown by open circles in figure 8. The results for τ_{31} are omitted here, because at low forward speed we have $\tau_{ij} = -\tau_{ji}$ $(i \neq j)$ (for more details, see Wu & Eatock Taylor (1988)). Some coefficients of the radiation load vary sharply in the vicinity of the critical frequency, which corresponds to $\bar{\sigma}^2 \approx 0.3906$ for the usual free surface. As shown in figure 5, the critical frequency decreases with increase

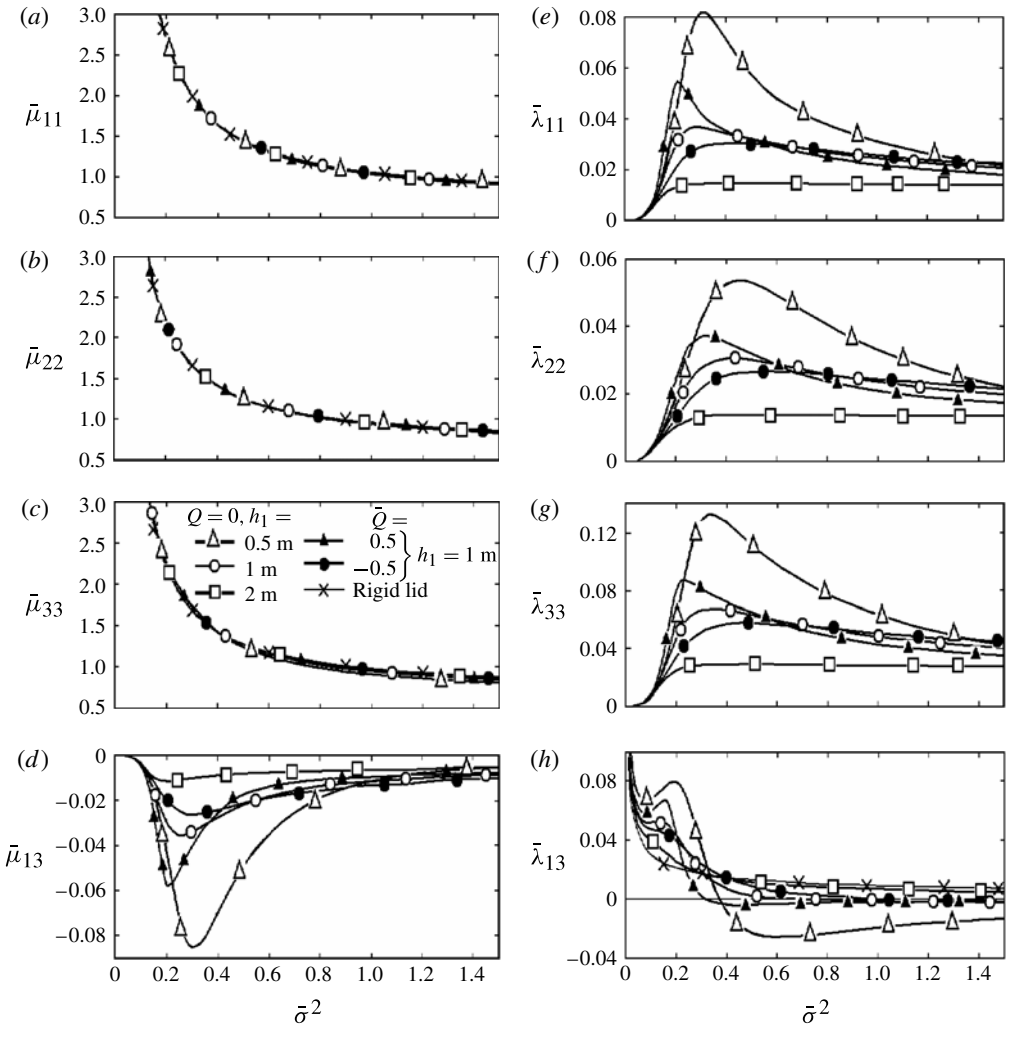

FIGURE 9. The radiation force at $\bar{u} = 0.4$ for an ice sheet: (*a*,*e*) surge, (*b*,*f*) sway, (*c*,*g*) heave, (*d*,*h*) surge–heave.

of the ice thickness for broken ice: $\bar{\sigma}^2 \approx 0.3460,\ 0.3146,\ 0.2712$ at $h_1 = 0.5,\ 1,\ 2$ m, respectively.

The effect of an ice sheet on the added-mass and damping coefficients is shown in figure 9. The radiation load is calculated at $\bar{u} = 0.4$ for different values of lateral stress and ice thickness: $Q = 0,\ h_1 = 0.5,\ 1,\ 2$ m, and $\bar{Q} = -0.5,\ 0.5,\ h_1 = 1$ m. For comparison, the values of the radiation force for a sphere submerged under a rigid lid are shown by the crosses in figure 9(*a*–*c*,*h*). At the rigid lid, the boundary condition for the radiation potentials ϕ_j $(j = 1, 2, 3)$ at $z = 0$ is used in a form similar to (5.1). Then we have $T_2/Z_2 = 1$ in (4.24), and

$$I_1(m, n, m', n') = -\frac{2\pi(n+n')!}{\varepsilon_m (2h)^{n+n'+1}}\delta_{mm'}, \quad I_2(m, n, m', n') = -\frac{\pi(n+n')!}{(\varepsilon_m - 1)(2h)^{n+n'+1}}\delta_{mm'} \quad (5.5)$$

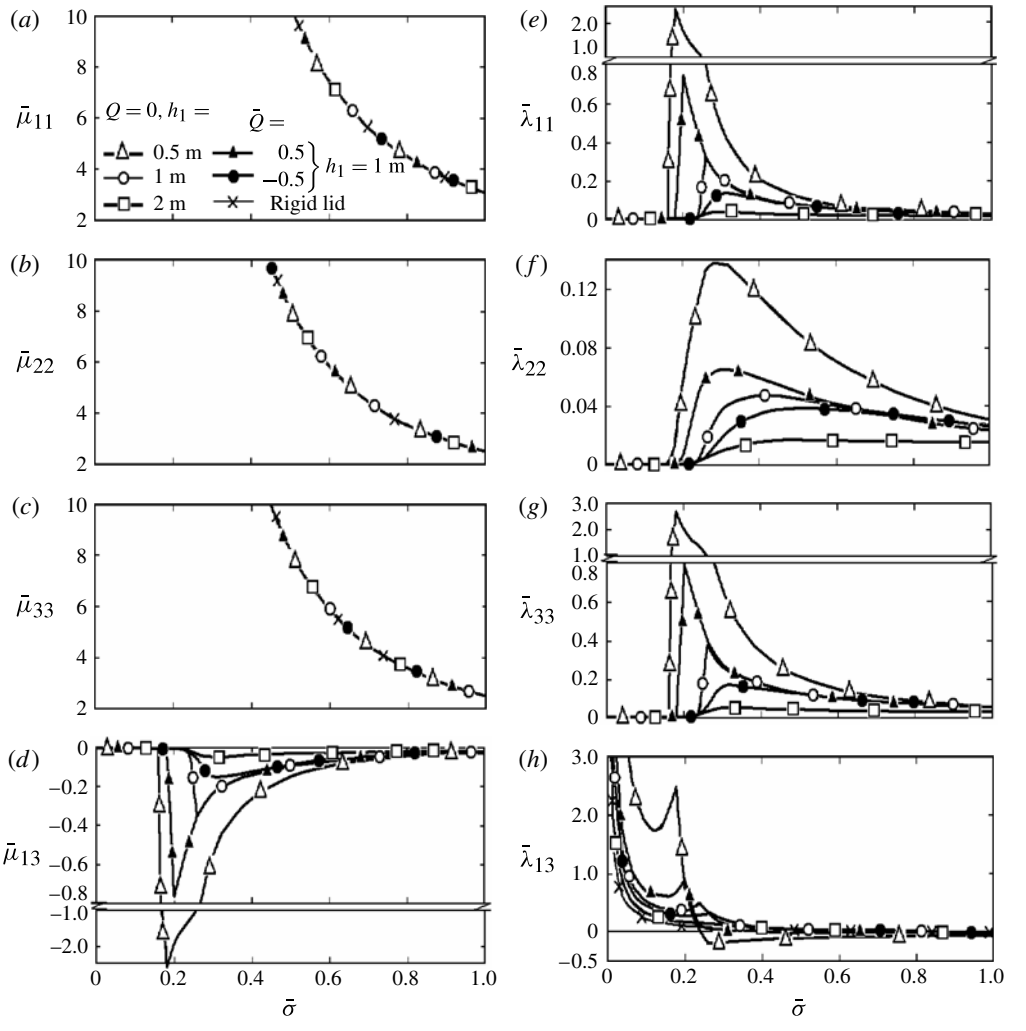

FIGURE 10. As figure 9, at $\bar{u} = 1$.

in (4.33) and (4.34), respectively. In this special case, only the diagonal added-mass coefficients μ_{jj} $(j = 1, 2, 3)$ and $\lambda_{13} = -\lambda_{31}$ are non-zero. We can see from figure 9 that the values of the diagonal added-mass coefficients for the ice sheet and the rigid lid are very close for all the parameters considered. However, for the value of the damping coefficient λ_{13}, the same effect is observed only at relatively thick ice cover with $h_1 = 2$ m. It should be noted that the radiation force in the case of an ice sheet is smaller than that in the case of broken ice at low forward speed. The value of forward speed $\bar{u} = 0.4$ is less than the minimum group velocity of the flexural–gravity waves for all the cases considered in figure 9 (cf. figure 2*d*). Consequently, the waves in the far field correspond only to the region G_4 in figure 4(*a*).

For a higher forward speed, $\bar{u} = 1$, the added-mass and damping coefficients are shown in figure 10. The radiation force is calculated for different values of ice thickness and lateral stress as in figure 9. In contrast to $\bar{u} = 0.4$, the value of the forward speed is now greater than the minimum group velocity for two

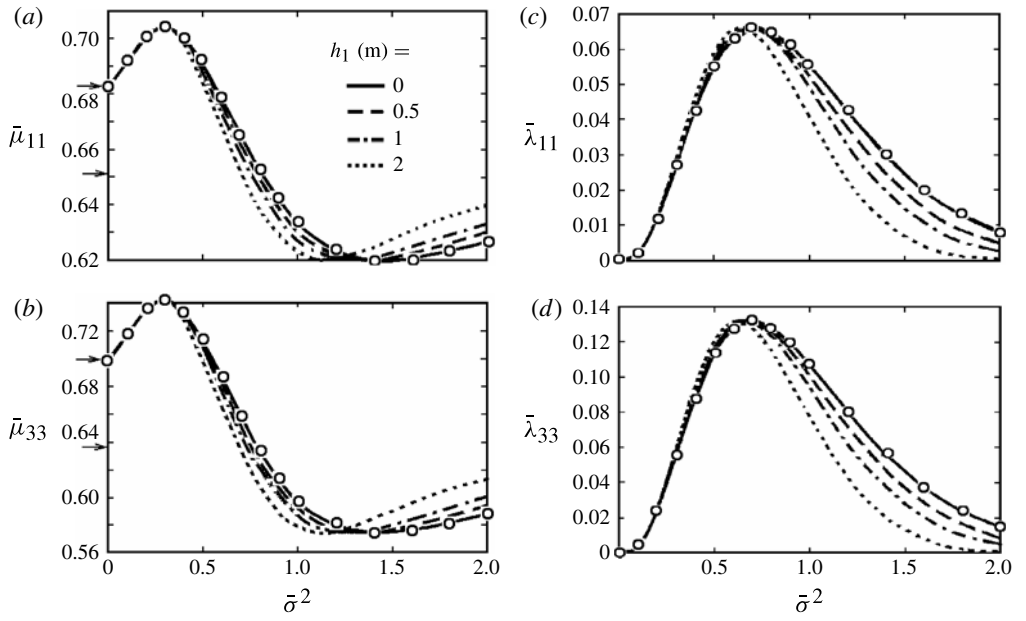

FIGURE 11. The radiation load at $u = 0$ for a free surface (solid lines) and for broken ice (dashed, dash-dotted and dotted lines) at $h_1 = 0.5,\ 1,\ 2$ m, respectively: (*a*,*c*) surge, (*b*,*d*) heave. Open circles correspond to the results by Wang (1986) for a free surface.

cases: $h_1 = 0.5$ m, $Q = 0$ ($\bar{U}_g \approx 0.7937$) and $h_1 = 1$ m, $\bar{Q} = 0.5$ ($\bar{U}_g \approx 0.7907$). In these cases, some components of the radiation force change sharply at frequencies that are close to the boundaries of the regions G_3 and G_4 in figure 4(*a*). These frequencies are $0.1751 < \bar{\sigma} < 0.2478$ at $h_1 = 0.5$ m, $Q = 0$ and $0.1969 < \bar{\sigma} < 0.2353$ at $h_1 = 1$ m, $\bar{Q} = 0.5$. At $h_1 = 1$ m, $Q = 0$, the value of the minimum group velocity is equal to $\bar{U}_g \approx 1.023$, which is very close to the value of the forward speed of the sphere. In this case, some components of the force change sharply in the vicinity of the critical frequency $\bar{\sigma}_* \approx 0.2433$. Similar to the case of low forward speed, the values of the diagonal added-mass coefficients for an ice sheet and a rigid lid are very close in the range of parameters considered. However, for the damping coefficient λ_{13}, similar behaviour is observed only at relatively thick ice cover with $h_1 = 2$ m.

As a particular case of the radiation problem with forward speed, we can take $u = 0$ and consider the radiation problem for the submerged sphere without forward speed. For this problem, the solution is significantly simplified and only the diagonal coefficients of the radiation force τ_{jj} ($j = 1, 2, 3$), with $\tau_{11} = \tau_{22}$, have non-zero values. The basic properties of the wave motion in the far field are given in § 3. Figure 11 shows the added-mass and damping coefficients for a sphere submerged under the usual free surface and under broken ice at different values of the ice thickness: $h_1 = 0.5,\ 1,\ 2$ m. The results for the free surface are compared with the values tabulated by Wang (1986), which are shown by open circles in figure 11. Good agreement is found. In figure 11(*a*,*b*), the horizontal arrows indicate the values of the added-mass coefficients $\bar{\mu}_{11}$ and $\bar{\mu}_{33}$, respectively, for two limiting cases: $\sigma \to 0$ ($\bar{\mu}_{11} \approx 0.6825$, $\bar{\mu}_{33} \approx 0.6985$) and $\sigma \to \infty$ ($\bar{\mu}_{11} \approx 0.6512$, $\bar{\mu}_{33} \approx 0.6360$). The first case corresponds to a rigid lid on the upper boundary of water, whereas

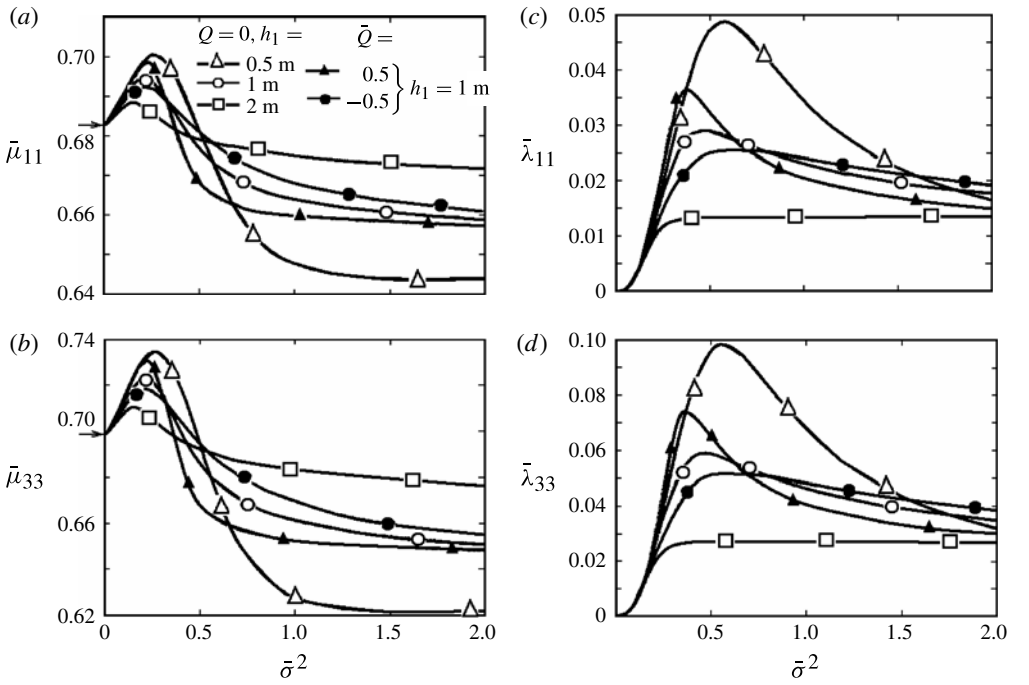

FIGURE 12. The radiation load for the ice sheet at $u = 0$: (*a*,*c*) surge, (*b*,*d*) heave.

the second corresponds to a weightless fluid with a free surface. The solutions of the radiation problem for these two cases can be easily obtained by the multipole expansion method, using the boundary conditions for the radiation potentials ϕ_j $(j = 1, 3)$ at $z = 0$ similar to (5.1) and (5.3), respectively. The approximate values of added-mass coefficients in these two cases are given in the reference book by Korotkin (2009, §§ 4.2.1 and 5.6.1, respectively). The wave motion is not generated in these cases and the damping coefficients λ_{11} and λ_{33} are equal to zero. It is interesting to note that the presence of broken ice on the upper boundary of the water does not produce a significant change of the extremum values of the radiation load but slightly shifts their positions towards lower frequencies.

The effect of an ice sheet on the added-mass and damping coefficients at $u = 0$ is shown in figure 12. The radiation force is calculated for different values of lateral stress and ice thickness: $Q = 0$, $h_1 = 0.5$, 1, 2 m, and $\bar{Q} = -0.5$, 0.5, $h_1 = 1$ m. At $\sigma \to 0$, the added-mass coefficients tend to the values for a rigid lid, which are shown by the horizontal arrows in figure 12(*a*,*b*). It is seen from figures 11 and 12 that the maximum values of the radiation force decrease with the ice thickness. Previously, the problem of wave radiation by a submerged sphere in deep water and in water of uniform finite depth with unstressed ice cover was considered by Das & Mandal (2008). All the curves for the added-mass and damping coefficients that were presented in that paper for deep water are confirmed fully using the present method. The numerical results obtained in the present paper suggest that an increase of the compression force (stretching stress) is equivalent to a decrease (increase) of the ice-cover thickness.

6. Conclusion

Within the framework of linearized theory, the velocity potential of an unsteady source has been derived for a fluid of infinite depth with an elastic solid cover. The cover is assumed to have a small thickness and uniform density. Taking into account the lateral stress imposed at the elastic cover makes it possible to consider the particular cases of an inertial surface, a flexible membrane, and a free surface with surface tension. The velocity potential for a source of arbitrary strength, starting from rest and moving along an arbitrary path, is derived first by solving an initial- and boundary-value problem using the Laplace transform. The result is similar in form to the transient source in a fluid with the usual free surface. An oscillating source with forward speed is derived from the transient source by specifying the appropriate strength and motion and considering the limiting case as time $t \to \infty$. The principal characteristics of the flexural–gravity waves in the far field are investigated with the method of stationary phase for double integrals.

As a sample application, a numerical solution of the radiation problem (surge, sway and heave) for water waves excited by a submerged sphere with forward speed is presented. The method of multipoles and the decomposition of the velocity potential in spherical harmonics are used to reduce the problem to the solution of an infinite system of linear equations. Numerical results are obtained for the hydrodynamic load acting on a submerged sphere that is moving in deep water with an ice cover. When the flexural rigidity and the density of the ice cover are taken to be zero, the numerical results for the hydrodynamic load for water with a free surface are recovered. It is shown that the hydrodynamic load acting on the submerged sphere depends significantly on its translating speed and the angular frequency as well as the thickness of the ice cover and its lateral stress. The solutions obtained can be used as a benchmark for the numerical methods developed for a submerged body of arbitrary shape. The approach proposed in this paper can be extended to the case of a fluid of finite depth.

Acknowledgements

I am grateful to the reviewers, whose constructive comments helped to improve the quality of the presentation.

Appendix

At $M = 0$, k_f can be obtained from (2.23) as

$$k_f^2 = (Q + \sqrt{Q^2 + 12g\rho D})/(6D). \tag{A 1}$$

At $Q = 0$, we have from this solution

$$k_f \left(\frac{D}{g\rho}\right)^{1/4} = 3^{-1/4} \approx 0.760, \quad U_f \left(\frac{\rho}{g^3 D}\right)^{1/8} = \frac{2}{27^{1/8}} \approx 1.325. \tag{A 2}$$

For a small stress, there is a nearly linear decrease of U_f with respect to Q (Schulkes *et al.* 1987)

$$U_f \approx 2\left(\frac{g^3 D}{27\rho}\right)^{1/8} \left(1 - \frac{3}{4}\varepsilon\right), \quad \varepsilon = \operatorname{arcsinh}\frac{Q}{\sqrt{12g\rho D}}. \tag{A 3}$$

For capillary–gravity waves ($D = M = 0, \quad Q = -T$), we have (e.g. Wehausen & Laitone 1960, p. 515)

$$k_f = \sqrt{g\rho/T}, \quad U_f = \sqrt{2}(gT/\rho)^{1/4}. \tag{A 4}$$

The explicit solutions for k_g and U_g can be obtained from (2.25) and (2.27) at $M = Q = 0$:

$$k_g\left(\frac{D}{g\rho}\right)^{1/4} = p \equiv \left(\frac{4}{\sqrt{15}} - 1\right)^{1/4} \approx 0.426, \quad U_g\left(\frac{\rho}{g^3 D}\right)^{1/8} = \frac{5p^4 + 1}{2\sqrt{p(p^4+1)}} \approx 0.878. \tag{A 5}$$

For capillary–gravity waves, we have

$$k_g\sqrt{\frac{T}{g\rho}} = \sqrt{\frac{2}{\sqrt{3}} - 1} \approx 0.393, \quad U_g\left(\frac{\rho}{gT}\right)^{1/4} = \frac{3^{3/8}(\sqrt{3}-1)}{\sqrt{2}(2-\sqrt{3})^{1/4}} \approx 1.086. \tag{A 6}$$

REFERENCES

BORN, M. & WOLF, E. 1964 *Principles of Optics*. Pergamon.

BUKATOV, A. E. 1980 Influence of a longitudinally compressed elastic plate on the non-stationary wave motion of a homogeneous liquid. *Fluid Dyn.* **15**, 687–693.

BUKATOV, A. E. & CHERKESOV, L. V. 1977 Unsteady oscillations of an elastic plate floating on the surface of the liquid stream. *Sov. Appl. Mech.* **13**, 103–107.

BUKATOV, A. E. & YAROSHENKO, A. A. 1986 Evolution of three-dimensional gravitationally warped waves during the movement of a pressure zone of variable intensity. *J. Appl. Mech. Tech. Phys.* **27**, 676–682.

BUKATOV, A. E. & ZHARKOV, V. V. 1997 Formation of the ice cover's flexural oscillations by action of surface and internal ship waves – Part I. Surface waves. *Intl J. Offshore Polar Engng* **7**, 1–12.

CHOWDHURY, R. G. & MANDAL, B. N. 2006 Motion due to fundamental singularities of finite depth water with an elastic solid cover. *Fluid Dyn. Res.* **38**, 224–240.

DAS, D. & MANDAL, B. N. 2006 Oblique wave scattering by a circular cylinder submerged beneath an ice-cover. *Intl J. Engng Sci.* **44**, 166–179.

DAS, D. & MANDAL, B. N. 2007 Wave scattering by a horizontal circular cylinder in a two-layer fluid with an ice-cover. *Intl J. Engng Sci.* **45**, 842–872.

DAS, D. & MANDAL, B. N. 2008 Water wave radiation by a sphere submerged in water with an ice-cover. *Arch. Appl. Mech.* **78**, 649–661.

DAS, D. & MANDAL, B. N. 2010 Wave radiation by a sphere submerged in a two-layer ocean with an ice-cover. *Appl. Ocean Res.* **32**, 358–366.

GRADSHTEYN, I. S. & RYZHIK, I. M. 1980 *Table of Integrals, Series, and Products*. Academic Press.

IL'ICHEV, A. T., SAVIN, A. A. & SAVIN, A. S. 2012 Formation of a wave on an ice-sheet above the dipole, moving in a fluid. *Dokl. Phys.* **57**, 202–205.

KHEYSIN, D. YE. 1967 *Dynamics of Floating Ice Cover*. Gidrometeoizdat, Leningrad (in Russian). Technical translation FSTC-HT-23-485-69, US Army Foreign Science and Technology Center.

KOROTKIN, A. I. 2009 *Added Masses of Ship Structures*, Fluid Mechanics and Its Applications, vol. 88. Springer.

KOZIN, V. M., CHIZHUMOV, S. D. & ZEMLYAK, V. L. 2010 Influence of ice conditions on the effectiveness of the resonant method of breaking ice cover by submarines. *J. Appl. Mech. Tech. Phys.* **51**, 398–404.

LU, D. Q. & DAI, S. Q. 2006 Generation of transient waves by impulsive disturbances in an inviscid fluid with an ice-cover. *Arch. Appl. Mech.* **76**, 49–63.

LU, D. Q. & DAI, S. Q. 2008*a* Flexural– and capillary–gravity waves due to fundamental singularities in an inviscid fluid of finite depth. *Intl J. Engng Sci.* **46**, 1183–1193.

LU, D. Q. & DAI, S. Q. 2008*b* Generation of unsteady waves by concentrated disturbances in an inviscid fluid with an inertial surface. *Acta Mech. Sin.* **24**, 267–275.

MOHAPATRA, S. & BORA, S. N. 2010 Radiation of water waves by a sphere in an ice-covered two-layer fluid of finite depth. *J. Adv. Res. Appl Math.* **2**, 46–63.

MOHAPATRA, S. & BORA, S. N. 2012 Exciting forces due to interaction of water waves with a submerged sphere in an ice-covered two-layer fluid of finite depth. *Appl. Ocean Res.* **34**, 187–197.

POGORELOVA, A. V., KOZIN, V. M. & ZEMLYAK, V. L. 2012 Motion of a slender body in a fluid under a floating plate. *J. Appl. Mech. Tech. Phys.* **53**, 27–37.

SAVIN, A. A. & SAVIN, A. S. 2012 Ice cover perturbation by a dipole in motion within a liquid. *Fluid Dyn.* **47**, 139–146.

SCHULKES, R. M. S. M., HOSKING, R. J. & SNEYD, A. D. 1987 Waves due to a steadily moving source on a floating ice plate. Part 2. *J. Fluid Mech.* **180**, 297–318.

SQUIRE, V. A. 2008 Synergies between VLFS hydroelasticity and sea-ice research. *Intl J. Offshore Polar Engng* **18**, 241–253.

SQUIRE, V. A., HOSKING, R. J., KERR, A. D. & LANGHORNE, P. J. 1996 *Moving Loads on Ice Plates*. Kluwer.

STUROVA, I. V. 2011 Hydrodynamic loads acting on an oscillating cylinder submerged in a stratified fluid with ice cover. *J. Appl. Mech. Tech. Phys.* **52**, 415–426.

STUROVA, I. V. 2012 The motion of a submerged sphere in a liquid under an ice sheet. *J. Appl. Math. Mech.* **76**, 293–301.

WANG, S. 1986 Motions of a spherical submarine in waves. *Ocean Engng* **13**, 249–271.

WEHAUSEN, J. V. & LAITONE, E. V. 1960 Surface waves. In *Handbuch der Physik,* vol. 9, pp. 446–778. Springer.

WU, G. X. 1995 Radiation and diffraction by a submerged sphere advancing in water waves of finite depth. *Proc. R. Soc. Lond.* A **448**, 29–54.

WU, G. X. & EATOCK TAYLOR, R. 1988 Radiation and diffraction of water waves by a submerged sphere at forward speed. *Proc. R. Soc. Lond.* A **417**, 433–461.

YEUNG, R. W. & KIM, J. W. 1998 Structural drag and deformation of a moving load on a floating plate. In *Proceedings of 2nd International Conference on Hydroelasticity in Marine Technology, Fukuoka, Japan*, pp. 77–88.